

Validation and results
from aircraft
campaigns

G. Allen et al.

This discussion paper is/has been under review for the journal Atmospheric Measurement Techniques (AMT). Please refer to the corresponding final paper in AMT if available.

Atmospheric composition and thermodynamic retrievals from the ARIES airborne TIR-FTS system – Part 2: Validation and results from aircraft campaigns

G. Allen¹, S. M. Illingworth¹, S. J. O'Shea¹, S. Newman², A. Vance²,
S. J.-B. Bauguitte³, F. Marengo², J. Kent², K. Bower¹, M. W. Gallagher¹,
J. Muller¹, C. J. Percival¹, C. Harlow², J. Lee⁴, and J. P. Taylor²

¹Centre for Atmospheric Science, University of Manchester, Manchester, M13 9PL, UK

²Met Office, Fitzroy Road, Exeter, EX1 3PB, UK

³Facility for Airborne Atmospheric Measurements, Cranfield, UK

⁴Centre for Atmospheric Science, University of York, York, UK

Received: 7 March 2014 – Accepted: 26 March 2014 – Published: 7 April 2014

Correspondence to: G. Allen (grant.allen@manchester.ac.uk)

Published by Copernicus Publications on behalf of the European Geosciences Union.

Title Page

Abstract

Introduction

Conclusions

References

Tables

Figures

⏪

⏩

◀

▶

Back

Close

Full Screen / Esc

Printer-friendly Version

Interactive Discussion



Abstract

This study validates trace gas and thermodynamic retrievals from nadir infrared spectroscopic measurements recorded by the UK Met Office Airborne Research Interferometer Evaluation System (ARIES) – a Thermal InfraRed Fourier Transform Spectrometer (TIR-FTS) on the UK Facility for Airborne Atmospheric Measurements (FAAM) BAe-146 aircraft.

Trace-gas-concentration and thermodynamic profiles have been retrieved and validated for this study throughout the troposphere and planetary boundary layer over a range of environmental variability using data from aircraft campaigns over and around London, the US Gulf Coast, and the Arctic Circle during the ClearLo, JAIVEX, and MAMM aircraft campaigns, respectively. Vertically-resolved retrievals of temperature and water vapour (H_2O), and partial-column retrievals of methane (CH_4), carbon monoxide (CO), and ozone (O_3), over both land and sea, were compared to corresponding measurements from high-precision in-situ analysers and dropsondes operated on the FAAM aircraft. Average Degrees of Freedom for Signal (DOFS) over a 0–9 km column range were found to be 4.97, 3.11, 0.91, 1.10, and 1.62 for temperature, H_2O , CH_4 , CO , and O_3 , respectively, when retrieved on 10 vertical levels. Partial column mean biases (and 1σ bias) averaged across all flight campaigns were $-0.4(\pm 1.9)\%$, $-6.0(\pm 13.1)\%$, $-0.6(\pm 2.1)\%$, $-3.0(\pm 18.4)\%$, and $+4.7(\pm 24.9)\%$, respectively, while the typical total a posteriori errors for individually retrieved profiles were 0.4 %, 9.5 %, 5.0 %, 21.2 %, and 15.0 %, respectively.

Averaging kernels derived for progressively lower altitudes show improving sensitivity to lower atmospheric layers when flying at lower altitudes. Temperature and H_2O display significant vertically resolved sensitivity throughout the column, whilst trace gases are usefully retrieved only as partial column quantities, with maximal sensitivity for trace gases other than H_2O within a layer 1 km and 2 km below the aircraft. This study demonstrates the valuable atmospheric composition information content that can be obtained by ARIES nadir TIR remote sensing for atmospheric process studies.

AMTD

7, 3397–3441, 2014

Validation and results from aircraft campaigns

G. Allen et al.

Title Page

Abstract

Introduction

Conclusions

References

Tables

Figures

◀

▶

◀

▶

Back

Close

Full Screen / Esc

Printer-friendly Version

Interactive Discussion



1 Introduction

In Part 1 of this study, Illingworth et al. (2013) discussed the theoretical and technical aspects of the retrieval methodology and a peripheral algorithm for atmospheric state retrievals from nadir thermal infrared spectra recorded by the Airborne Research Interferometer Evaluation System (ARIES, see below). Illingworth et al. (2013) reviewed how airborne remote sensing of the atmosphere can be used to derive important compositional and thermodynamic data for monitoring and modelling applications, and how such datasets can complement satellite retrievals (typically at lower spatial resolution) and high accuracy (but point-specific) in situ measurements to aid regional process studies. In summary, airborne remote sensing can help to bridge the gap between spatial extremes locally and regionally through their ability to observe wide (and selectable) fields of view and to perform targeted sampling; for example through manoeuvring in the vertical.

Illingworth et al. (2013), described and characterised the Manchester Airborne Retrieval Scheme (MARS), a configurable system tailored for the optimally-estimated retrieval of atmospheric composition from infrared spectra recorded by the ARIES open-path-FTS instrument (described in detail by Wilson et al., 1999) flown on the UK Facility for Airborne Atmospheric Measurements (FAAM) BAe-146 aircraft. The ARIES is an analogue of the Infrared Atmospheric Sounding Interferometer (IASI) flown on the MetOp-A and B satellites, both having an apodised spectral resolution of $\sim 0.5 \text{ cm}^{-1}$ between 4 and $16 \mu\text{m}$. No further description of the ARIES and retrieval formalism will be given here and readers are referred to Illingworth et al. (2013) and references therein for details.

We focus here on the validation of operationally-retrieved profiles of temperature, water vapour (H_2O), methane (CH_4), carbon monoxide (CO), and ozone (O_3), which will be referred to collectively as the retrieval products hereafter. In this paper, validation refers to the statistical and profile-by-profile comparison of retrieved data with their in-situ counterpart, both directly, and after convolution with retrieval-specific ARIES

AMTD

7, 3397–3441, 2014

Validation and results from aircraft campaigns

G. Allen et al.

Title Page

Abstract

Introduction

Conclusions

References

Tables

Figures



Back

Close

Full Screen / Esc

Printer-friendly Version

Interactive Discussion



Validation and results from aircraft campaigns

G. Allen et al.

Title Page

Abstract

Introduction

Conclusions

References

Tables

Figures



Back

Close

Full Screen / Esc

Printer-friendly Version

Interactive Discussion



averaging kernels. For the trace gases, partial columns will be compared due to their constrained vertical resolvability (see Sect. 3). We will report the performance of operational retrievals from ARIES spectra across a range of environments, using airborne in situ measurements for the purpose of validation for each location. For context and later comparison, we now briefly discuss example validation studies of the retrieval products of concern to this study for three example infrared remote sensing instruments on satellite, airborne and ground-based platforms.

The Total Column Carbon Observing Network (TCCON) is a network of ground-based, sun-viewing, near-IR, Fourier transform spectrometers that has been established to measure greenhouse gases as total column Dry Molar Fractions (DMFs). Since its inception in 2004, the TCCON network has grown to include 18 sites globally, and currently produces DMFs of H₂O, CO₂, CO, CH₄, and other trace gases (Wunch, 2011). Due to cited systematic biases in the spectroscopy, the absolute accuracy of the column measurements is quoted as ~ 1 %, however this can be improved by calibrating them to the World Meteorological Organization (WMO) in situ trace gas measurement scales, using profiles obtained with in situ instrumentation flown on aircraft over the TCCON sites (Wunch, 2010). After this calibration, the precision of the DMFs retrieved from single spectra improves significantly, and is about 0.15 % for CO₂, 0.2 % for CH₄, and up to 0.5 % for CO (Toon, 2009).

The Methane Airborne MAPper (MAMAP) is an airborne spectrometer system designed to make measurements of dry air partial columns of CO₂ and CH₄ on small spatial scales with a precision of better than 2 % (Gerilowski, 2011). MAMAP operates with a ground pixel resolution of approximately 29 m × 33 m for a typical aircraft altitude of 1250 m and a velocity of 200 km h⁻¹. The main uncertainties in the retrieval were noted to arise from potential inaccuracies in the calculation of the solar zenith angle and the surface elevation of the scene. Such uncertainties (important in the visible and near-infrared) are not expected in the thermal infrared. Krings et al. (2011) reported that by using a CH₄ proxy method (in which the retrieved CH₄ is used to account for the light path modification by simultaneously retrieving alongside CO₂), the total

uncertainty estimate was reduced to 0.24 % in a standard individual column retrieval of CO₂.

The IASI has an Instantaneous Field of View (IFOV) that is approximately 12 km in diameter at nadir (Blumstein et al., 2004). Depending on the trace gas and the retrieval scheme employed, IASI can provide weakly resolved vertical profiles, with the number of independent pieces of information for each gas depending mostly on the thermal state of the atmosphere (e.g. 1–2 for CO in the troposphere, and 3–5 for O₃ up to 0.1 hPa, Hilton, 2012). Using an Optimal Estimation Method (OEM) developed by Coheur et al. (2005), Boynard et al. (2009), showed that on average, IASI O₃ retrievals exhibit a consistent positive bias of about 3 % compared to ground-based measurements. Similarly, Illingworth et al. (2011) showed that on average, total tropospheric column CO retrievals from IASI exhibit a positive bias of approximately 3 % when compared to modelled data. Despite small biases in comparison to other datasets, IASI retrieved products also have large associated uncertainties for individually retrieved profiles, where the dominant term is typically caused by the smoothing of the continuous atmosphere by the retrieval schemes, which necessarily assume a discretized atmosphere. Illingworth et al. (2011) noted that typical smoothing uncertainty for IASI total tropospheric columns range from 18 % to 34 %.

The brief discussion above demonstrates the relative limitations and benefits of remote sensing measurements within the troposphere from viewpoints below, within and far above it. Each has specific weighting in terms of sensitivity to different layers within the tropospheric column and each has different uncertainties. We highlight here how aircraft remote sensing can help to bridge spatial sampling scales between ground-based and satellite platforms, whilst high precision in situ data can be simultaneously provided (where equipped) to routinely validate and calibrate retrievals.

The remainder of this manuscript is structured as follows: in Sect. 2, we will describe the validating measurements used for this study; Sect. 3 describes the validation flight campaigns where ARIES was operated; and Sect. 4 compares operational retrievals with in situ measurements.

**Validation and results
from aircraft
campaigns**

G. Allen et al.

Title Page

Abstract

Introduction

Conclusions

References

Tables

Figures



Back

Close

Full Screen / Esc

Printer-friendly Version

Interactive Discussion



2 Data sources

Measured data discussed in this paper were recorded using instrumentation on board the BAe146-301 atmospheric research aircraft. In this section, we describe the aircraft platform and in situ instrumentation used here for validation. Only relevant FAAM in-situ instrumentation that record measurements corresponding to the retrieval products are introduced here.

2.1 The BAe146 platform

The BAe-146-301 atmospheric research aircraft is operated by Directflight Ltd and managed by FAAM, which is a joint entity of the Natural Environment Research Council (NERC) and the UK Met Office. This four-engine jet plane is modified for research use and capable of up to 5 h duration with a scientific payload of up to 4000 kg. In situ instrumentation described in Sect. 2.1 sampled ambient air inside the converted passenger cabin. This air was fed by purpose-built rearward facing window-mounted inlets (O'Shea et al., 2013). Typical air speed and aircraft pitch angle on science runs were around 115 ms^{-1} and $+4.5^\circ$ respectively. The GPS position, aircraft orientation, and velocity were all sampled at 50 Hz, and recorded at 32 Hz by an Applanix POS AV 510 GPS-aided Inertial Navigation (GIN) unit.

2.2 Trace gas and thermodynamic measurements

Thermodynamic and trace gas instruments on the BAe-146 used for this study are listed in Table 1. A 5-hole turbulence probe mounted on the aircraft nose was used in conjunction with the GIN system to provide 3-D wind fields and high frequency (32 Hz) turbulence measurements. Thermodynamic instruments include a General Eastern GE 1011B Chilled Mirror Hygrometer, measuring dew-point temperature, and a Rosemount/Goodrich type-102 True Air Temperature sensor, which recorded data at 32 Hz using a non-de-iced Rosemount 102AL platinum resistance immersion thermometer,

AMTD

7, 3397–3441, 2014

Validation and results from aircraft campaigns

G. Allen et al.

Title Page

Abstract

Introduction

Conclusions

References

Tables

Figures

◀

▶

◀

▶

Back

Close

Full Screen / Esc

Printer-friendly Version

Interactive Discussion



mounted outside of the boundary layer of the aircraft near the nose. The turbulence probe also used measurements from the GIN and measurements of the ambient air temperature to correct for kinetic effects.

Carbon monoxide was measured at 1 Hz by an AL5002 Fast CO Monitor using a UV fluorescence methodology, as described by Gerbig et al. (1999); the instrument was regularly calibrated (once every 30 min) in flight against certified standards. Ozone was recorded at 1 Hz by a TECO 49C UV photometer, and the transmission time from the exterior to the instrument via the sampling line can be assumed to be negligible (less than the 1 s integration time for these in situ sensors). These instruments are core to the aircraft fit, and are used regularly in a variety of FAAM campaigns. Therefore, the accuracy of the reported O₃ and CO concentrations has been regularly assessed by intercomparisons with ground-based instruments and equivalent instrumentation on other aircraft. In those comparisons, both CO and O₃ have been found to be consistently accurate to within 5 ppb across a range of typical atmospheric concentrations (e.g. as compared with instrumentation on the NSF C-130 aircraft reported in Allen et al., 2011). This compares favourably with the reported instrument precision of 1 % above the instrument limits of detection, which are ~ 20 ppb and 5 ppb for CO and O₃, respectively.

The CH₄ observations on board the FAAM BAe-146 were made using a cavity-enhanced absorption spectrometer. This system is based on a commercially available analyser (Fast Greenhouse Gas Analyser, Model RMT- 200) from Los Gatos Research Inc., USA, which has been modified for airborne operation (O'Shea et al., 2013). Calibration curves are determined in-flight using three WMO traceable standards, with accuracy/bias estimated at no more than 1.28 ppb for CH₄ (with 1σ precision of 2.48 ppb at 1 Hz). Measurements are reported as dry air mole fractions.

In addition to the in situ instrumentation, for some of the flights in this study Vaisala RD93 dropsondes were released from the aircraft, from high altitude and when over the sea. The RD93 is a general-purpose dropsonde for high-altitude deployment from a variety of aircraft. Slowed in its descent through the atmosphere by a special parachute,

Validation and results from aircraft campaigns

G. Allen et al.

Title Page

Abstract

Introduction

Conclusions

References

Tables

Figures

◀

▶

◀

▶

Back

Close

Full Screen / Esc

Printer-friendly Version

Interactive Discussion



Validation and results from aircraft campaigns

G. Allen et al.

Title Page

Abstract

Introduction

Conclusions

References

Tables

Figures

◀

▶

◀

▶

Back

Close

Full Screen / Esc

Printer-friendly Version

Interactive Discussion



the RD93 measures the atmospheric profiles of pressure, temperature, relative humidity and wind from the point of launch to the ground. The RD93 transmits meteorological data via a 400 MHz meteorological band telemetry link to the receiving system on-board the aircraft, with an on-board GPS receiver tracking the dropsonde horizontal movement as it is borne by the wind. The manufacturer-specified accuracies of the RD93 are 0.2 K, 0.4 hPa, and 2 % for temperature, pressure and relative humidity, respectively.

2.3 Cloud and aerosol lidar

A mini-lidar cloud system on the FAAM aircraft has also been used here to test for successful cloud screening of the ARIES data (see Sect. 4). The mini-lidar is a Leosphere (Model ALS450) elastic backscattering system with daytime capability, suitable for aerosol and cloud observations, and features a depolarization channel. Its operational wavelength is 355 nm and it is mounted in a nadir-viewing geometry. For more details about the mini-Lidar instrument, see Marengo et al. (2011).

3 FAAM campaigns used for validation

For validation purposes, we have chosen to use well-characterised datasets from several FAAM aircraft campaigns, conducted in diverse locations to capture the typical natural variability of composition and thermodynamic backgrounds across the range of environments in which the FAAM aircraft typically samples. The campaigns that were chosen for this study were: the Joint Airborne IASI Validation Experiment (JAIVEx); the Clean air for London (ClearfLo) study; and the Methane and other greenhouse gases in the Arctic – Measurements, process studies and Modelling (MAMM) project. These campaigns were based around the US Gulf Coast, London and the Arctic Circle, respectively, and are described in more detail below.

3.1 JAIVEx

The JAIVEx campaign was a calibration-validation campaign which used ARIES radiance data to radiometrically validate the IASI instrument. It was conducted over the Gulf of Mexico and operated out of Houston, USA, during April–May 2007. For an overview of the JAIVEx mission, see Larar et al. (2010) and for a full discussion of the performance of ARIES during the JAIVEx project, see Newman et al. (2012). In addition to temperature, water vapour and trace gas concentrations (see Sect. 2.2), the FAAM aircraft released dropsondes, which sampled the atmospheric thermodynamic structure below the aircraft at high spatial resolution (~ 6 m), which will also be used here for validation. We present data collected during flight B290 during JAIVEX, which took place on the morning of 30 April 2007 over the Gulf of Mexico. The B290 flight track and profile are shown in Fig. 1. Take-off time from Houston Airport was 12:45 UTC (07:45 LT) and landing time at New Orleans was 17:20 UTC (12:20 LT).

The Gulf of Mexico area and the operational area of the aircraft were mostly cloud-free on 30 April 2007, as observed in-flight and from GOES satellite cloud imagery (not shown). This makes this flight an ideal case study for nadir remote sensing validation, where cloudy scenes would otherwise prevent retrieval by MARS. Indeed, this area at this time of year was chosen for its climatologically low cloud fraction to facilitate this IASI calibration-validation mission.

Two extended periods (of between 30 min and 1 h in duration) at cruising altitudes of 7.3 km and 9 km were conducted. These are the northwest-southeast and northeast-southwest transects seen in Fig. 1, respectively. At these altitudes, the instantaneous ground footprint of ARIES due to the instrument's 44 mrad circular field of view (full angle) has a radius of ~ 161 m, and 198 m, representing an instantaneous footprint area of ~ 0.08 km² and 0.12 km², respectively. The exact footprint of the ARIES retrievals is then a product of both this instantaneous footprint, and the ground-track of the aircraft integrated over the ARIES sampling/integration time (5 s in this case).

AMTD

7, 3397–3441, 2014

Validation and results from aircraft campaigns

G. Allen et al.

Title Page

Abstract

Introduction

Conclusions

References

Tables

Figures



Back

Close

Full Screen / Esc

Printer-friendly Version

Interactive Discussion



3.2 ClearfLo

The Clean air for London (ClearfLo) project was conceived to provide long-term integrated measurements of the meteorology and composition of London's urban atmosphere, recorded at street level and at elevated sites, and complemented by modelling to improve and characterise predictive capability for air quality. A separate but synergistic FAAM airborne project took place during July and August 2012, consisting of five 5 h flights during which the ARIES and in situ trace gas instrumentation was operated to record measurements in a wide area around and centred on London (see Fig. 2). Repeated sampling was targeted on the downwind London plume and upwind background inflow; a detailed description of the ClearfLo campaign is given by Bohnenstengel (2012).

For validation, we have used data from flights B724 and B725, both conducted between 10:00 and 16:30 UTC for both 30 July 2012 and 9 August 2012, representing relatively clean and polluted cases, respectively, and characterised by well-mixed Atlantic westerly maritime inflow in the former and stagnant air (high pressure) in the latter. This contrast is useful for validation to characterise the ability to retrieve information in clean and polluted environments. Flight tracks for these two flights can be seen as the thick (B724) and thin (B725) traces in Fig. 2. In both flights, air upwind of London was seen to be less polluted than air downwind in the situ measurements (see Sect. 4).

3.3 MAMM

The MAMM project aims to improve quantitative knowledge of Arctic CH₄ and other gases from various sources, whilst also determining their magnitudes and spatial distributions. The FAAM component of this mission involved three separate flying campaigns within the Arctic Circle: July 2012, August 2013, and September 2013. In this study we have used data from the July 2012 period during two flights: B719 and B720, on 17 July 2012 and 18 July 2012, respectively, conducted between 09:00 UTC and

AMTD

7, 3397–3441, 2014

Validation and results from aircraft campaigns

G. Allen et al.

Title Page

Abstract

Introduction

Conclusions

References

Tables

Figures



Back

Close

Full Screen / Esc

Printer-friendly Version

Interactive Discussion



Validation and results from aircraft campaigns

G. Allen et al.

Title Page

Abstract

Introduction

Conclusions

References

Tables

Figures



Back

Close

Full Screen / Esc

Printer-friendly Version

Interactive Discussion



16:00 UTC. The former was conducted over the wetlands of western Finland and the latter predominantly over the Norwegian Sea between the coasts of Norway and Svalbard (see Fig. 3). These two flights provide contrast between sea and land retrievals in an otherwise similar natural environment, thereby allowing us to examine potential sources of systematic bias associated with surface type. The spiral ascent pattern seen in Fig. 3 near 27° E, 68° N flown during B720 was centred on the Sodankylä TCCON site, however cloudy conditions on this day prevented a direct comparison with TCCON CH₄ and CO₂ measurements. The in situ measurements recorded during this spiral provide the vertical profiles we have used for retrieval validation with in situ data for this flight.

4 Results and discussion

The results of the validation using the FAAM dataset outlined in Sect. 2.3 are now presented and discussed. To illustrate typical examples for individual retrievals we show retrieval metrics of spectral fit and residual, averaging kernels, and sources of total-and-component a posteriori retrieval error for profiles chosen from one flight for each of the retrieved parameters where comparable in situ data exists. We then present a statistical interpretation of the whole validation dataset across selected flights in terms of mean bias and uncertainty for the entire dataset (i.e. across all campaigns). The spectral window and co-retrieved state vectors for each nominal parameter (described further in Part 1 of this study) is given in Table 2. The ARIES spectra were co-added over 5 s of sampling time (10 scans) in all retrievals considered here and retrievals were all performed on 10 vertical levels unless otherwise stated.

4.1 Cloud detection and screening performance

We have tested a cloud-detection scheme based on the brightness temperature difference in a window and non-window spectral region (described further by Illingworth

smaller biases (less than 500 ppm) seen in the light-blue profiles in Fig. 5a retrieved from ~ 3 km flight altitude. In all retrievals shown in Fig. 5a, the retrieval represents an improvement on the a priori profile.

Figure 5b shows the flight-mean profiles, binned into 10 equidistant altitude layers, for the retrieved (red) and in-situ (black) data along with the in-situ profile convolved with the mean ARIES AK (green) for the flight. The convolved profile is defined as $x_a + A(x - x_a)$, where A is the averaging kernel, x is the retrieved profile and x_a is the a priori profile. It should be noted that we would expect there to be natural variability in the retrieval scene during a flight and that some of the variability seen in the retrievals reflects this, but by comparing the mean of the retrievals with the mean of the in situ data across the entire flight, we can compare a more consistent dataset than we would by comparing individual profiles. Due to the varying flight altitude, the mean retrieved and convolved profile represents a weighted mean reflecting the different sampling frequency within each altitude bin.

Also shown in Fig. 5b are bars that represent the standard deviation of retrieved and in situ data at each profile level which were calculated from the distribution of retrievals for the flight. This should not be confused with the a posteriori error associated with individual retrievals, which is reported separately in Table 3. The AK-convolved in situ profile (green) compares well with the mean retrieved profile (red), with the latter overlapping well within the corresponding 1σ of the dropsonde measurements. This shows that the retrieval agrees well with an idealised retrieval scheme giving confidence in the optimal performance of the MARS. The mean bias in Fig. 5a ranges between 110 ppm (1 %) at 500 m and ~ 1140 ppm (14 %) at 3 km. The increased bias at 3 km is due to the poorer performance of the retrievals from higher altitude which dominate the contribution to the mean profile at this altitude (yellow profiles in Fig. 5a), whereas the profiles recorded from an altitude just below 3 km (light blue in Fig. 5a) do capture the locally drier layer between 2.5 km and 3 km. In summary, there is information content in vertically-resolved water vapour nadir retrievals from ARIES and fine vertical structure can be resolved in the layers nearest to the observer (within ~ 2 km).

Validation and results from aircraft campaigns

G. Allen et al.

Title Page

Abstract

Introduction

Conclusions

References

Tables

Figures

◀

▶

◀

▶

Back

Close

Full Screen / Esc

Printer-friendly Version

Interactive Discussion



**Validation and results
from aircraft
campaigns**

G. Allen et al.

Title Page

Abstract

Introduction

Conclusions

References

Tables

Figures

◀

▶

◀

▶

Back

Close

Full Screen / Esc

Printer-friendly Version

Interactive Discussion



Q-branch and its strong sensitivity to temperature makes it very sensitive to the effects of vertical discretisation necessary for the radiative transfer modelling, and as such, some error may be expected. However, the P and R branches of this band, which are likewise sensitive to temperature, but which do not saturate over path-lengths similar to the thickness of the layers used here (~ 600 m), provide the bulk of the measurement information in this spectral window. This is precisely why CO_2 and temperature are simultaneously retrieved. There are also two weak unidentified potential absorption lines in the measured spectrum at 740 cm^{-1} and 746 cm^{-1} . However, the overall residual is commensurate with the ARIES radiometric uncertainty (black dotted lines in Fig. 6b). The effect of this is also implicit to the a posteriori error calculation, which is consistently $\sim 0.8\text{ K}$ across the profile and dominated by the smoothing and measurement uncertainty terms (Fig. 6d).

The temperature AKs (Fig. 6c) for this example demonstrate excellent vertical resolution with a DOFS value of 4.73, which compares with the simulated (idealised) DOFS of ~ 4 in Part 1 of this study. The AK peak at each altitude is only slightly dependent on information content from other levels and is typically smoothed over a 1 km length (when using 10 levels at 9 km flight altitude). This result confirms that vertically-resolved tropospheric profiles of temperature can be usefully reported using MARS for ARIES measured spectra. This capability is especially useful for atmospheric process studies such as boundary layer transport and outflow, where knowledge of the thermodynamic structure of the lower atmosphere is important.

Figure 7 shows temperature retrievals for 103 individual profiles across flight B290 (Fig. 7a) and the weighted mean flight profiles together with their in situ counterparts (Fig. 7b) in the same manner as that presented for water vapour in Fig. 5. This flight was chosen as there were four dropsondes released over various locations along the flight track and we were interested in how MARS might respond to the presence of temperature inversions in the real atmosphere. Figure 7a shows that the retrieved temperature profiles (blue) were consistently negatively biased relative to dropsonde data between 2.5 km and 4 km by up to 5 K at peak. This compares with a negative bias in

Validation and results from aircraft campaigns

G. Allen et al.

Title Page

Abstract

Introduction

Conclusions

References

Tables

Figures



Back

Close

Full Screen / Esc

Printer-friendly Version

Interactive Discussion



(Fig. 8b). The AKs for methane (Fig. 8c) demonstrate significantly less vertical resolution than for H₂O or temperature with a DOFS value of 0.86, which compares with the typical simulated DOFS for CH₄ of ~ 1.0 predicted in Part 1 of this study at similar altitudes. There is clearly more sensitivity to the upper layers of the column (between 5 km and 8 km); however information in these layers is noted to be strongly influenced by the layers below. On inspection of the spectrally-resolved weighting function for CH₄ (not shown) it can be seen that this arises because of saturation of strong CH₄ absorption lines with the remainder of the lower layer information coming from much weaker lines and a commensurately reduced signal-to-noise. This is also typical of IASI retrievals of methane in the troposphere, which likewise show limited penetration and sensitivity into the tropospheric column, and confirms that only partial columns can be usefully reported for ARIES retrievals. It is also important to note that this partial column information is mainly weighted to a 2 km layer below the aircraft.

The total a posteriori error (Fig. 8d) on independent retrievals is significant at ~ 100 ppb (~ 5%) of in situ concentration across the profile, which is again dominated by the smoothing and measurement (radiometric uncertainty) components.

Figure 9a shows 389 methane concentration retrievals (coloured profiles) from flight B725, compared to vertically binned (averaged into 10 equidistant layers across the profile) in situ concentration profiles measured by the FGGA (black). Firstly, we note that the a priori (operationally derived from the MACC database (see Inness et al., 2013 and Part 1 of this study for details) in blue shows a significant negative bias relative to in situ data of around 3% (~ 60 ppb at all altitudes). Despite this, the retrieved profiles tend well toward the in-situ data in all cases and the a posteriori error bars (dotted lines in Fig. 9a) always overlap the in situ profile. When averaged across a flight, Fig. 9b shows good agreement between retrieval and in situ data in the flight-averaged profiles between 2.5 km and 9 km, but shows a clear negative bias (up to ~ 2.5%) in the lowest layers (below 2 km). This is due to the lack of near-surface sensitivity noted from the AK in Fig. 8c, meaning that the retrieval in those layers tends toward a negatively biased a priori. Partial-column comparisons (see Table 3 and Fig. 9b) for B725

**Validation and results
from aircraft
campaigns**

G. Allen et al.

Title Page

Abstract

Introduction

Conclusions

References

Tables

Figures

◀

▶

◀

▶

Back

Close

Full Screen / Esc

Printer-friendly Version

Interactive Discussion



constraint in MARS. Figure 12a and b show CO mean-flight retrievals for two other flights – B720 and B724, from the MAMM and ClearLo campaigns, respectively. For those flights, we tested the performance of MARS with a 25 % a priori covariance for each retrieval level (note the wider blue bars in Fig. 12 compared to Fig. 11b). When using this relaxed constraint, and despite the positively biased a priori, we observe much better retrieval performance in the mean for altitudes above 2 km when comparing the in situ profile and that convolved with the ARIES AK (black and green lines respectively). For these two flights we see a mean partial column bias of -3% and -2% respectively, with a corresponding 1σ of 19 % and 22 %, respectively. This compares to natural sampled variability of 8 % and 12 %, respectively (see Table 3). Given the small overall mean bias (-3% , 3.3 ppb) in Table 3 compared to the overall natural variability of CO measured in the atmosphere (17 %, 17.6 ppb), which also compares to the variability in the bias (20 %, 20.4 ppb), we can be confident the a posteriori error from individual profiles is a conservative uncertainty for retrievals here; this is $\sim 21\%$ of the partial column (see Table 3), which compares favourably to the upper IASI uncertainties of 34 % reported by Illingworth et al. (2011).

4.6 Ozone

Figure 13 shows convergence parameters for example O_3 retrievals over Northern Sweden at 8.3 km flight altitude during flight B719 during the MAMM campaign on 21 July 2012. We see a largely featureless residual comparable within the instrumental radiometric uncertainty (Fig. 13b). The AK shows little vertical resolution and a sensitivity weighted to a layer ~ 3 km below the aircraft (Fig. 13c). Total a posteriori error is ~ 17 ppb ($\sim 25\%$ in this example) across the profile and dominated by the smoothing term (80 % of total error), with the measurement error term contributing $\sim 20\%$ to the total error (Fig. 8d).

We also show results for flight B724 as a special contrasting case. Figure 14a shows 42 O_3 retrievals from flight B724 (ClearLo) compared to vertically-binned in situ concentration profile measured by the 2B Technologies instrument (black). The a priori

(operationally derived from the MACC database in this case), has little bias below 7 km but appears to misrepresent the presence of stratospheric air enriched in ozone above 7 km (confirmed also by the aircraft-measured potential temperature profile, not shown). Meteorological charts for this day show a tropopause fold over the area (not shown) – a mesoscale feature not commonly captured by coarse-scale global circulation models such as those employed for MACC. This makes this case study particularly interesting in assessing the performance of MARS to unexpected events. Encouragingly, the retrieved profiles in Fig. 14 do capture some of the (vertically smoothed) structure of this stratospheric intrusion despite the a priori constraint above 7 km. The AK at 7.1 km (Fig. 13c) contains dominant peaks from both that layer and the two adjacent layers (8.95 and 5.61 km), and this smoothing is manifest in the retrieved profile as a positive and negative bias in the layers around a rapidly increasing gradient in ozone at 7 km. This is analogous to the retrieval response to the presence of a strong temperature inversion discussed in Sect. 4.3 and shows that MARS can capture important (and unexpected) vertical gradients in ozone within 2 km of the aircraft altitude.

Comparing the B724 flight-mean and in situ partial columns (Fig. 14b and Table 3) we see a mean bias of +3.7% and 1σ of this bias of $\pm 17\%$ (22.4 ppb), compared to a natural variability of $\pm 8\%$. Figure 14b shows the mean bias standard error (red bars) and we see that this overlaps well within the 1σ in situ bars (black).

Due to the potential of the FAAM aircraft to routinely sample stratospheric air, two further flight examples are shown (Fig. 15) for incidences and absences of stratospheric intrusion during flights B720 (MAMM, Fig. 15a), and B290 (JAIVEx, Fig. 15b), respectively. In both examples, the retrieval performs well and captures smoothed vertical structure in the layers within 3 km below the aircraft. In these flights, mean partial column biases were found to be +5.4% and +8.1% with 1σ of the bias equal to 20% and 13% respectively (Table 3). This compares to natural variability of 17% and 21%, respectively. Global dataset bias can be summarised as being small compared to natural variability, which itself is comparable to the bias-standard-deviation. This suggests that bias cannot be distinguished from natural variability and therefore that (as for the other

Validation and results from aircraft campaigns

G. Allen et al.

Title Page

Abstract

Introduction

Conclusions

References

Tables

Figures



Back

Close

Full Screen / Esc

Printer-friendly Version

Interactive Discussion



Validation and results from aircraft campaigns

G. Allen et al.

[Title Page](#)
[Abstract](#)
[Introduction](#)
[Conclusions](#)
[References](#)
[Tables](#)
[Figures](#)




[Back](#)
[Close](#)
[Full Screen / Esc](#)
[Printer-friendly Version](#)
[Interactive Discussion](#)


Visser, S., Whalley, L. K., Williams, L. R., Xu, L., Young, D. E., and Zotter, P.: Meteorology, air quality, and health in London: the ClearLo project, *B. Am. Meteorol. Soc.*, in press, 2014.

Boynard, A., Clerbaux, C., Coheur, P.-F., Hurtmans, D., Turquety, S., George, M., Hadji-Lazaro, J., Keim, C., and Meyer-Arnek, J.: Measurements of total and tropospheric ozone from IASI: comparison with correlative satellite, ground-based and ozonesonde observations, *Atmos. Chem. Phys.*, 9, 6255–6271, doi:10.5194/acp-9-6255-2009, 2009.

Coheur, P. F., Barret, B., Turquety, S., Hurtmans, D., Hadji-Lazaro, J., and Clerbaux, C.: Retrieval and characterization of ozone vertical profiles from a thermal infrared nadir sounder, *J. Geophys. Res.-Atmos.*, 110, D24303, doi:10.1029/2005JD005845, 2005.

Gerilowski, K., Tretner, A., Krings, T., Buchwitz, M., Bertagnolio, P. P., Belemezov, F., Erzinger, J., Burrows, J. P., and Bovensmann, H.: MAMAP – a new spectrometer system for column-averaged methane and carbon dioxide observations from aircraft: instrument description and performance analysis, *Atmos. Meas. Tech.*, 4, 215–243, doi:10.5194/amt-4-215-2011, 2011.

Hilton, F., Armante, R., August, T., Barnet, C., Bouchard, A., Camy-Peyret, C., and Hurtmans, D.: Hyperspectral Earth observation from IASI: five years of accomplishments, *B. Am. Meteorol. Soc.*, 93, 347–370, doi:10.1175/BAMS-D-11-00027.1, 2012.

Illingworth, S. M., Remedios, J. J., Boesch, H., Moore, D. P., Sembhi, H., Dudhia, A., and Walker, J. C.: ULIRS, an optimal estimation retrieval scheme for carbon monoxide using IASI spectral radiances: sensitivity analysis, error budget and simulations, *Atmos. Meas. Tech.*, 4, 269–288, doi:10.5194/amt-4-269-2011, 2011.

Illingworth, S. M., Allen, G., Newman, S., Vance, A., Marenco, F., Harlow, R. C., Taylor, J., Moore, D. P., and Remedios, J. J.: Atmospheric composition and thermodynamic retrievals from the ARIES airborne FTS system – Part 1: Technical aspects and simulated capability, *Atmos. Meas. Tech. Discuss.*, 6, 10833–10887, doi:10.5194/amtd-6-10833-2013, 2013.

Inness, A., Baier, F., Benedetti, A., Bouarar, I., Chabrilat, S., Clark, H., Clerbaux, C., Coheur, P., Engelen, R. J., Errera, Q., Flemming, J., George, M., Granier, C., Hadji-Lazaro, J., Huijnen, V., Hurtmans, D., Jones, L., Kaiser, J. W., Kapsomenakis, J., Lefever, K., Leitão, J., Razinger, M., Richter, A., Schultz, M. G., Simmons, A. J., Suttie, M., Stein, O., Thépaut, J.-N., Thouret, V., Vrekoussis, M., Zerefos, C., and the MACC team: The MACC reanalysis: an 8 yr data set of atmospheric composition, *Atmos. Chem. Phys.*, 13, 4073–4109, doi:10.5194/acp-13-4073-2013, 2013.

Validation and results from aircraft campaigns

G. Allen et al.

[Title Page](#)
[Abstract](#)
[Introduction](#)
[Conclusions](#)
[References](#)
[Tables](#)
[Figures](#)




[Back](#)
[Close](#)
[Full Screen / Esc](#)
[Printer-friendly Version](#)
[Interactive Discussion](#)


Krings, T., Gerilowski, K., Buchwitz, M., Reuter, M., Tretner, A., Erzinger, J., Heinze, D., Pflüger, U., Burrows, J. P., and Bovensmann, H.: MAMAP – a new spectrometer system for column-averaged methane and carbon dioxide observations from aircraft: retrieval algorithm and first inversions for point source emission rates, *Atmos. Meas. Tech.*, 4, 1735–1758, doi:10.5194/amt-4-1735-2011, 2011.

Larar, A. M., Smith, W. L., Zhou, D. K., Liu, X., Revercomb, H., Taylor, J. P., Newman, S. M., and Schlüssel, P.: IASI spectral radiance validation inter-comparisons: case study assessment from the JAIVEx field campaign, *Atmos. Chem. Phys.*, 10, 411–430, doi:10.5194/acp-10-411-2010, 2010.

Marenco, F. and Hogan, R. J.: Determining the contribution of volcanic ash and boundary layer aerosol in backscatter lidar returns: a three component atmosphere approach, *J. Geophys. Res.-Atmos.*, 116, D00U06, doi:10.1029/2010JD015415, 2011.

Newman, S. M., Larar, A. M., Smith, W. L., Ptashnik, I. V., Jones, R. L., Mead, M. I., Revercomb, H., Tobin, D. C., Taylor, J. K., and Taylor, J. P.: The Joint Airborne IASI Validation Experiment: an evaluation of instrument and algorithms, *J. Quant. Spectrosc. Ra.*, 11, 1372–1390, 2012.

O'Shea, S. J., Bauguitte, S. J.-B., Gallagher, M. W., Lowry, D., and Percival, C. J.: Development of a cavity-enhanced absorption spectrometer for airborne measurements of CH₄ and CO₂, *Atmos. Meas. Tech.*, 6, 1095–1109, doi:10.5194/amt-6-1095-2013, 2013.

Rothman, L. S., Gordon, I. E., Babikov, Y., Barbe, A., Chris Benner, D., Bernath, P. F., Birk, M., Bizzocchi, L., Boudon, V., Brown, L. R., Campargue, A., Chance, K., Cohen, E. A., Coudert, L. H., Devi, V. M., Drouin, B. J., Fayt, A., Flaud, J.-M., Gamache, R. R., Harrison, J. J., Hartmann, J.-M., Hill, C., Hodges, J. T., Jacquemart, D., Jolly, A., Lamouroux, J., Le Roy, R. J., Li, G., Long, D. A., Lyulin, O. M., Mackie, C. J., Massie, S. T., Mikhailenko, S., Müller, H. S. P., Naumenko, O. V., Nikitin, A. V., Orphal, J., Perevalov, V., Perrin, A., Polovtseva, E. R., Richard, C., Smith, M. A. H., Starikova, E., Sung, K., Tashkun, S., Tennyson, J., Toon, G. C., Tyuterev, G., and Wagner, G.: The HITRAN2012 molecular spectroscopic database, *J. Quant. Spectrosc. Ra.*, 130, 4–50, doi:10.1016/j.jqsrt.2013.07.002, 2013.

Toon, G., Blavier, J. F., Washenfelder, R., Wunch, D., Keppel-Aleks, G., Wennberg, P., and Notholt, J.: Total column carbon observing network (TCCON), in: *Fourier Transform Spectroscopy* (p. JMA3), Optical Society of America, 2009.

Wilson, S., Atkinson, N., and Smith, J.: The development of an airborne infrared interferometer for meteorological sounding studies, *J. Atmos. Ocean. Tech.*, 16, 1912–1927, 1999.

**Validation and results
from aircraft
campaigns**

G. Allen et al.

Title Page

Abstract

Introduction

Conclusions

References

Tables

Figures



Back

Close

Full Screen / Esc

Printer-friendly Version

Interactive Discussion



Wunch, D., Toon, G. C., Wennberg, P. O., Wofsy, S. C., Stephens, B. B., Fischer, M. L.,
Uchino, O., Abshire, J. B., Bernath, P., Biraud, S. C., Blavier, J.-F. L., Boone, C., Bow-
man, K. P., Browell, E. V., Campos, T., Connor, B. J., Daube, B. C., Deutscher, N. M., Diao, M.,
Elkins, J. W., Gerbig, C., Gottlieb, E., Griffith, D. W. T., Hurst, D. F., Jiménez, R., Keppel-
Aleks, G., Kort, E. A., Macatangay, R., Machida, T., Matsueda, H., Moore, F., Morino, I.,
5 Park, S., Robinson, J., Roehl, C. M., Sawa, Y., Sherlock, V., Sweeney, C., Tanaka, T., and
Zondlo, M. A.: Calibration of the Total Carbon Column Observing Network using aircraft pro-
file data, *Atmos. Meas. Tech.*, 3, 1351–1362, doi:10.5194/amt-3-1351-2010, 2010.

Wunch, D., Toon, G. C., Blavier, J.-F. L., Washenfelder, R. A., Notholt, J., Connor, B. J. Grif-
fith, D. W. T., Sherlock, V., and Wennberg, P. O.: The total carbon column observing network,
10 *Philos. T. R. Soc. A*, 369, 2087–2112, 2011.

Validation and results from aircraft campaigns

G. Allen et al.

Table 1. BAe-146 thermodynamic and trace gas instruments used in this study. T , P and RH refer to ambient temperature, pressure and relative humidity, respectively.

Instrument	Technique	Parameter	Reference/Company
Aerolaser AL5002	Fluorescence	CO	Aero-Laser GmbH, Gerbig et al. (1999)
2B Technologies 202 ozone analyser	UV absorption	O ₃	2B Technologies Inc
Los Gatos FGGA	Cavity enhanced absorption spectroscopy	CH ₄ , CO ₂	Los Gatos Inc., O'Shea et al. (2013)
Aerodyne QCLAS	Quantum Cascade Laser absorption Spectroscopy	CH ₄ , N ₂ O	Aerodyne Inc.
General Eastern GE 1011B Hygrometer	Chilled mirror dewpoint	H ₂ O	General Eastern Inc.
Rosemount/Goodrich type 102	Thermistor	T	Rosemount Aerospace Inc.
Airborne Vertical Atmospheric Profiler System (AVAPS)	Drosonde + GPS	T , P , RH, winds	Vaisala Inc
Mini Lidar Leosphere ALS450	Lidar	Cloud and aerosol	Leosphere Inc; Marenco et al. (2011)

Title Page

Abstract

Introduction

Conclusions

References

Tables

Figures

◀

▶

◀

▶

Back

Close

Full Screen / Esc

Printer-friendly Version

Interactive Discussion



Validation and results from aircraft campaigns

G. Allen et al.

Table 2. Retrieval parameters and associated spectral windows and co-retrieved parameters.

Retrieval Parameter	Spectral Window	Co-retrieved parameters
T	690–775 cm^{-1}	T_s , H ₂ O, Aerosol extinction, CO ₂
H ₂ O	1200–1410 cm^{-1}	T_s , H ₂ O, Aerosol extinction
CH ₄	1240–1290 cm^{-1}	T_s , H ₂ O, Aerosol extinction
O ₃	990–1040 cm^{-1}	T_s , H ₂ O, Aerosol extinction
CO	2143–2181 cm^{-1}	T_s , H ₂ O, Aerosol extinction

Title Page

Abstract

Introduction

Conclusions

References

Tables

Figures

◀

▶

◀

▶

Back

Close

Full Screen / Esc

Printer-friendly Version

Interactive Discussion



Validation and results from aircraft campaigns

G. Allen et al.

Table 3. Summary of retrieval metrics and validation results across all flights. Numbered from left to right columns show: (1) target parameter, (2) FAAM flight number, (3) number of ARIES (4) retrievals, mean degrees of freedom for signal, (5) flight-mean column-averaged a posteriori error; (6) mean bias of retrieved partial columns relative to in situ data; (7) the standard deviation of biases for all individual retrievals for each flight; and (8) the standard deviation of the corresponding in situ data. For each parameter, a global weighted mean is shown in bold. For columns 4 through 8, units are K for T , ppm for H_2O , and ppb for other gases (percentages in parentheses are relative to the mean retrieved partial column).

Param	Flight	N	DOFS	$\overline{\epsilon}_p$	Mean Bias	σ_{bias}	σ_{true}
T	B290	209	4.97	0.8(0.3%)	-0.4(0.2%)	1.9	2.5
	B720	41	3.89	1.1(0.5%)	-1.3(0.6%)	1.5	1.2
	B724	27	4.73	0.9(0.4%)	-1.1(0.5%)	2.1	2.8
	B725	125	4.89	0.8(0.3%)	-0.7(0.3%)	1.9	1.9
	All	402	4.71	0.9(0.4%)	-0.7(0.3%)	1.9	2.1
H_2O	B290	203	3.34	1132(5.1%)	-910(4.4%)	1030	500
	B720	41	2.45	1320(13%)	+560(5.7%)	760	690
	B724	20	3.19	876(6%)	-650(4.9%)	1540	1500
	B725	125	3.16	954(9.1%)	-270(2.8%)	1680	1470
	All	389	3.11	1144(9.5%)	-479(4.8%)	1111	775
CH_4	B719	14	0.91	97(5.0%)	-45(2.7%)	67.6	21.1
	B720	24	0.89	99(5.1%)	+21(1.1%)	63.2	5.5
	B724	20	0.86	101(5.1%)	-29(1.5%)	19.3	12.9
	B725	389	0.97	85(4.5%)	-11(0.6%)	40.1	15.2
	All	447	0.91	96(5.0%)	-11.2(0.6%)	41.3	14.8
CO	B290	203	1.14	25(17%)	-2.2(2%)	17.1	41.4
	B719	41	0.91	22(25%)	-1.0(1.3%)	13.2	7.0
	B720	41	0.97	18(18%)	-3.2(3%)	19.2	8.0
	B724	30	0.98	21(20%)	-2.0(2%)	22.4	12.1
	B725	110	1.17	20(17%)	-6.3(6%)	30.2	11.3
All	425	1.10	23(21.2%)	-3.3(3%)	20.4	17.6	
O_3	B290	191	1.81	15(23%)	+8.1(12%)	9.0	13.8
	B719	41	1.34	17(25%)	+4.0(6.0%)	14.9	12.1
	B720	58	1.72	15(19%)	+4.4(5.4%)	16.3	14.7
	B724	42	1.83	12(13%)	+3.3(3.7%)	31.2	10.9
	B725	25	1.40	17(24%)	-2.2(3.0%)	22.1	18.9
All	357	1.62	11(15%)	+3.5(4.7%)	18.7	14.1	

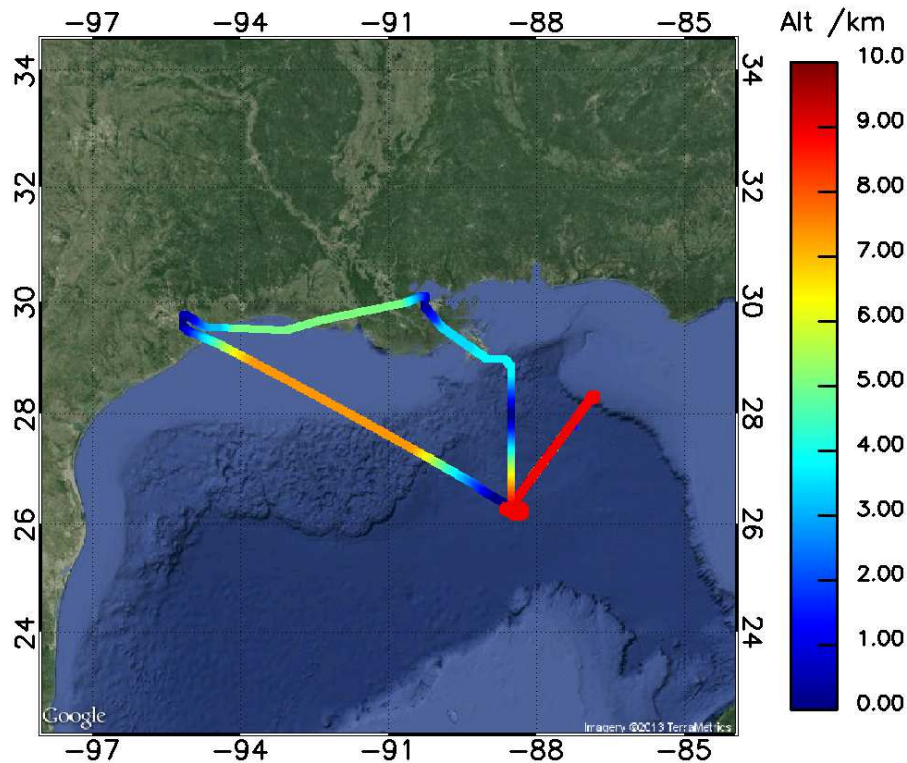


Fig. 1. Flight track of FAAM flight B290 on 30 April 2007 over the Gulf of Mexico, colour-coded for altitude as indicated in the legend. Permission granted by Google Maps and Terrametrics, Inc to display the imagery shown here.

Validation and results
from aircraft
campaigns

G. Allen et al.

Title Page

Abstract

Introduction

Conclusions

References

Tables

Figures

◀

▶

◀

▶

Back

Close

Full Screen / Esc

Printer-friendly Version

Interactive Discussion



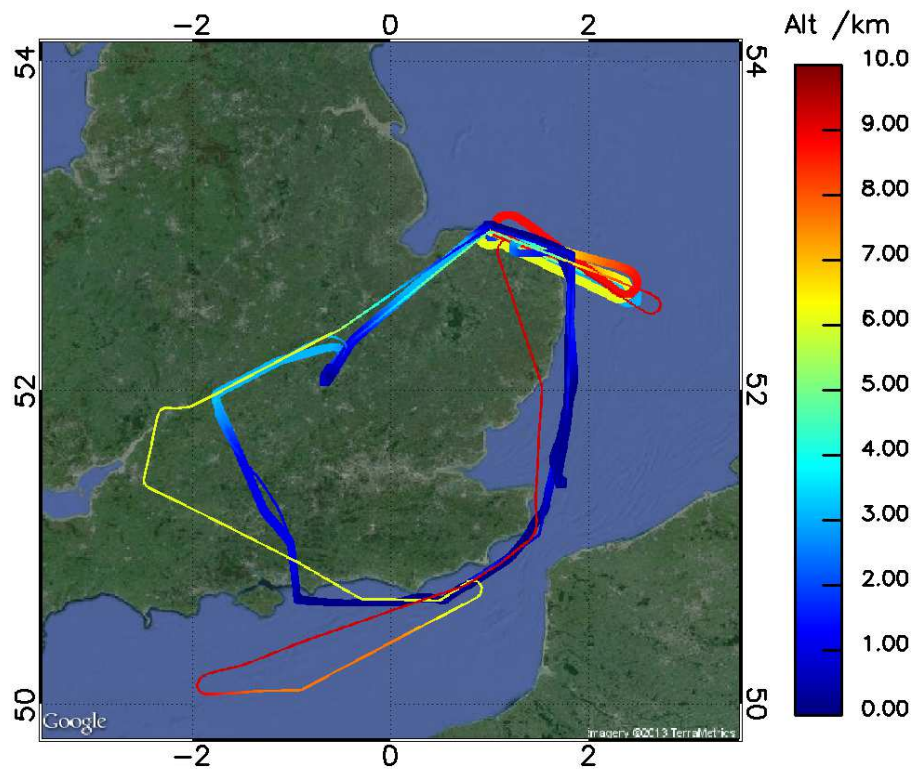


Fig. 2. Flight track of FAAM flights B724 (thick track) and B725 (thin track) on 30 July 2012 and 9 August 2012 respectively, and colour-coded for altitude as indicated in the legend. Permission granted by Terrametrics, Inc to display the imagery shown here.

Validation and results from aircraft campaigns

G. Allen et al.

Title Page	
Abstract	Introduction
Conclusions	References
Tables	Figures
◀	▶
◀	▶
Back	Close
Full Screen / Esc	
Printer-friendly Version	
Interactive Discussion	



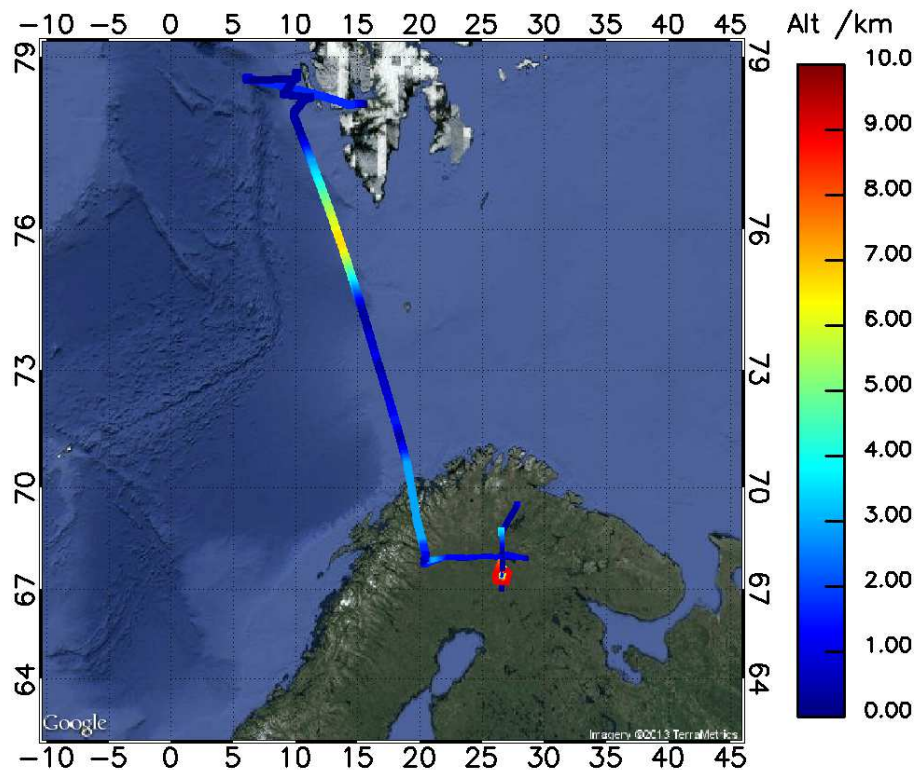


Fig. 3. Flight track of FAAM flights B719 (thick track) and B720 (thin track) on 17 July 2012 and 18 July 2012 respectively, and colour-coded for altitude as indicated in the legend. Permission granted by Google Maps and TerraMetrics, Inc to display the imagery shown here.

Validation and results
from aircraft
campaigns

G. Allen et al.

Title Page

Abstract

Introduction

Conclusions

References

Tables

Figures

◀

▶

◀

▶

Back

Close

Full Screen / Esc

Printer-friendly Version

Interactive Discussion



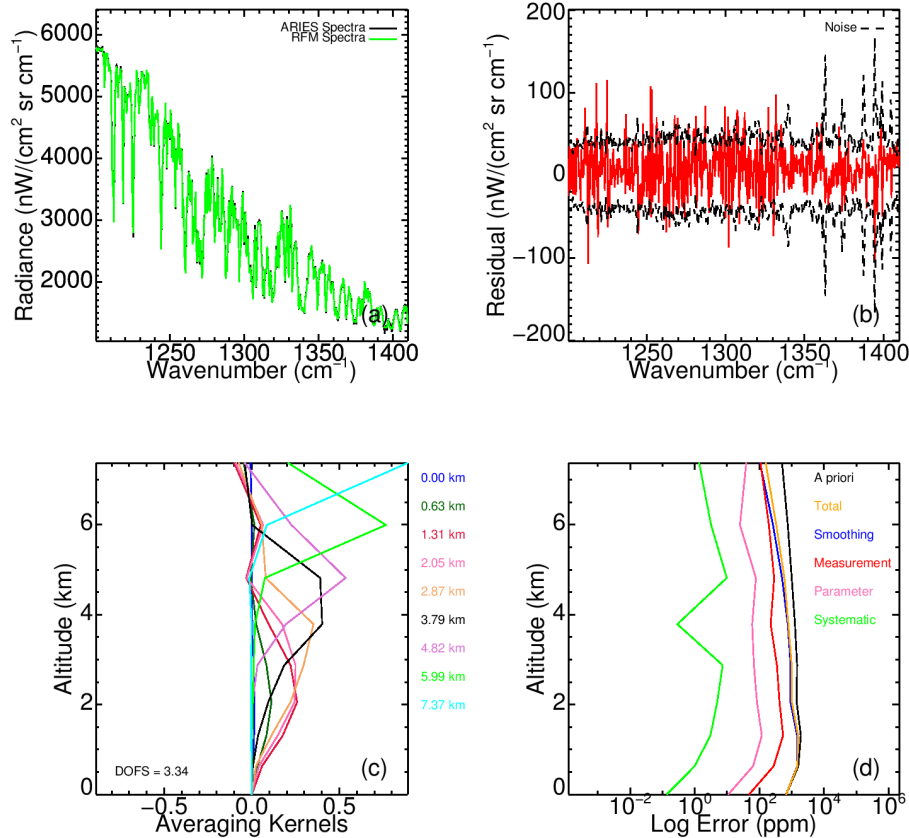


Fig. 4. Example retrieval metrics for H₂O during flight B290 over the Gulf of Mexico at 7.4 km altitude showing: **(a)** measured (ARIES, black) and fitted (green) spectra; **(b)** residual difference between the ARIES-measured and fitted spectrum (red) and noise-equivalent spectral radiance (NESR, black); **(c)** averaging kernels (and degrees of freedom for signal, inset); **(d)** total and component systematic and random error components.

Validation and results from aircraft campaigns

G. Allen et al.

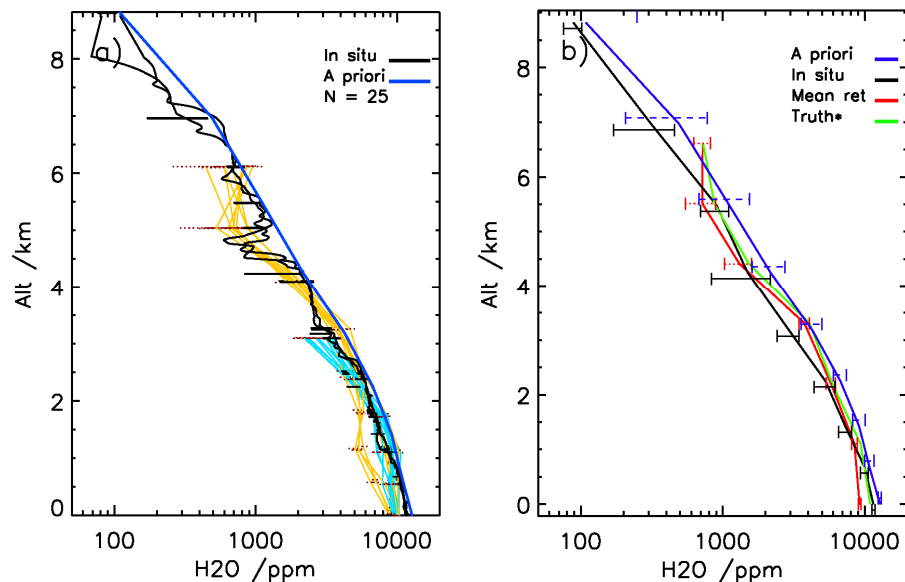


Fig. 5. Retrievals and comparison to in situ data for: **(a)** water vapour retrieval concentration profiles for flight B725, colour-coded for flight altitude (light blue corresponds to 3 km, orange to 6.1 km). Retrieval uncertainty is shown as the dotted red bars for each profile. In situ dropsonde (black) and a priori profiles (blue) are also shown; **(b)** mean profiles from flight B725 for: retrieved (red), in-situ-measured (black), in-situ average convolved with ARIES averaging kernels (green); and a priori (blue). Standard error for the mean retrieved profiles and the a priori uncertainty are shown as correspondingly coloured bars at each vertical level.

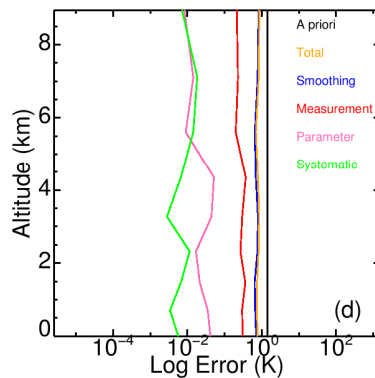
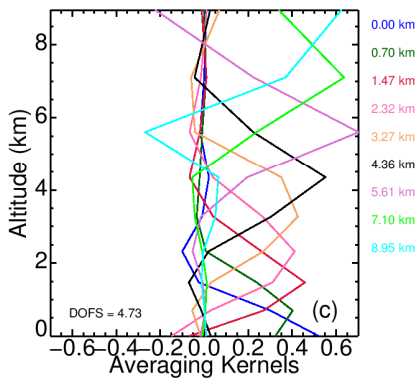
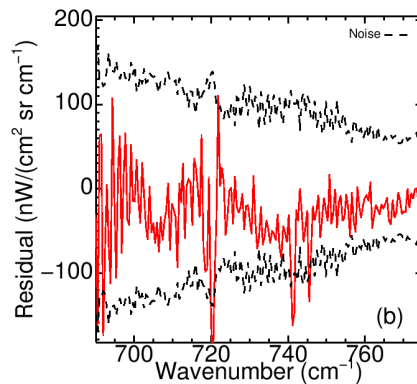
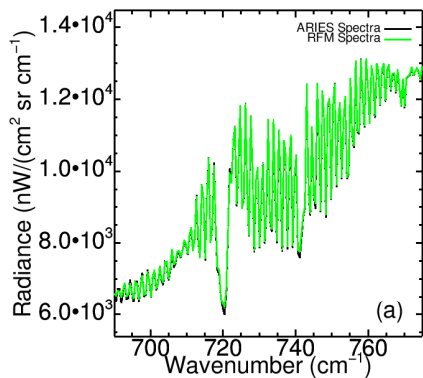


Fig. 6. Example retrieval metrics for temperature during flight B724 over land at 8.9 km altitude showing: **(a)** measured (ARIES) and fitted spectra; **(b)** residual difference between the ARIES-measured spectrum and fitted spectrum; **(c)** averaging kernels (and degrees of freedom for signal, inset); **(d)** total and component systematic and random error components.

Validation and results from aircraft campaigns

G. Allen et al.

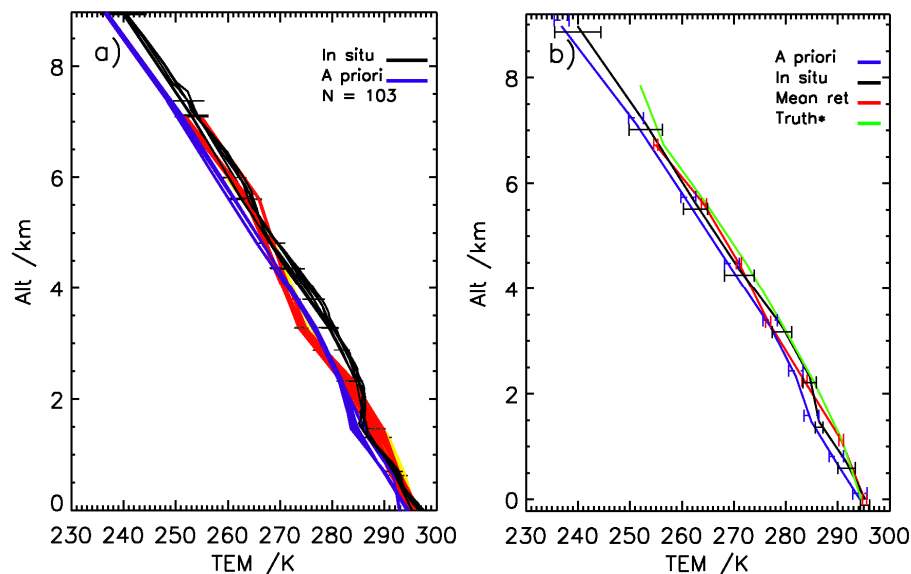


Fig. 7. (a) 103 individual temperature retrieval profiles across flight B290 colour-coded for observer (flight) altitude. Retrieval uncertainty is shown as the dotted red bars for each profile. In situ dropsonde (black) and a priori profiles (blue) are also shown; and (b) mean profiles from flight B290 for: retrieved (red), in-situ-measured (black), in-situ average convolved with ARIES averaging kernels (green); and a priori (blue). Standard error for the mean retrieved profiles and the priori uncertainty are shown as correspondingly coloured bars at each vertical level.

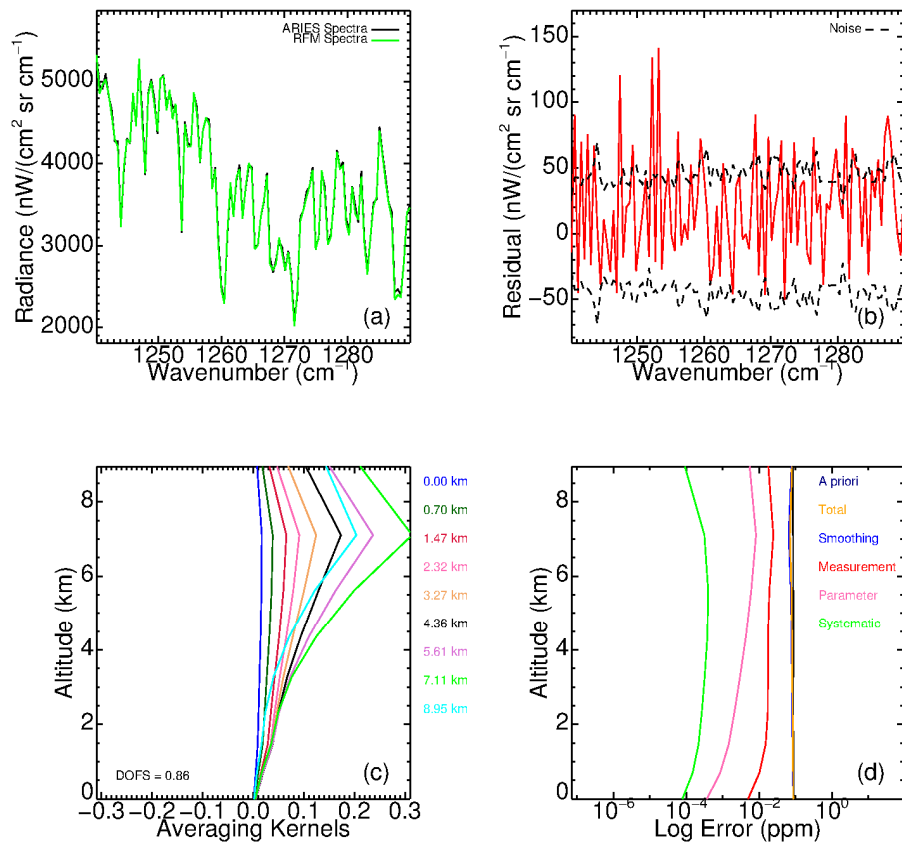


Fig. 8. Example retrieval metrics for CH₄ during flight B724 over land at 9.0 km altitude showing: **(a)** measured (ARIES) and fitted spectra; **(b)** residual difference between the ARIES-measured spectrum and fitted spectrum; **(c)** averaging kernels (and degrees of freedom for signal, inset); **(d)** total and component systematic and random error components.

Validation and results from aircraft campaigns

G. Allen et al.

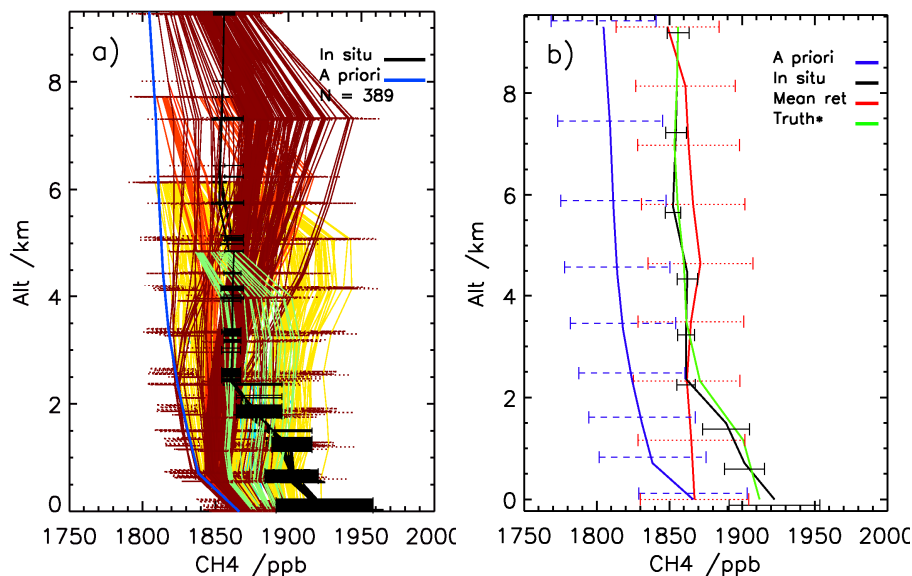


Fig. 9. (a) 389 individual methane concentration retrieval profiles across flight B725 colour-coded for observer (flight) altitude (red = 8.7 km, yellow = 6.1 km, green = 4.8 km). Retrieval uncertainty (total error) is shown as the dotted bars in each case. In situ and a priori profiles are also shown as per legend; (b) mean profiles from flight B725 for: retrieved (red), in-situ-measured (black), in-situ average convolved with ARIES averaging kernels (green); and a priori (blue). Standard deviations of the measurement variability and a priori are shown as correspondingly-coloured bars at each binned vertical level and the root mean square retrieval uncertainty (total error) is shown by the red bars.

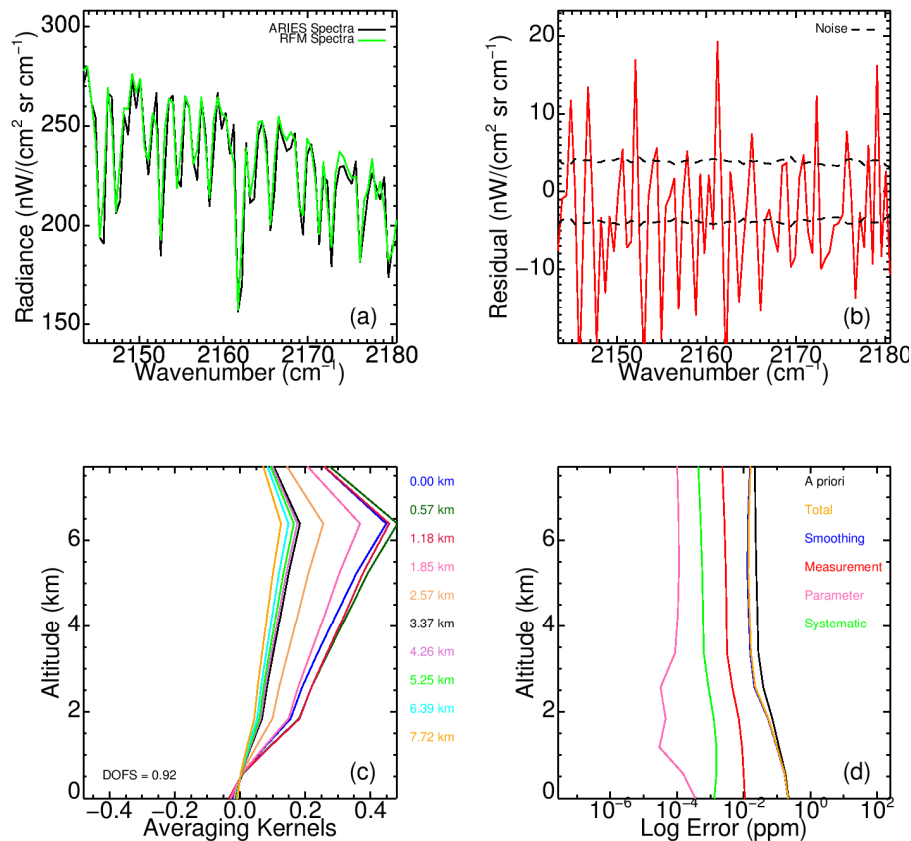


Fig. 10. Example retrieval metrics for CO during flight B725 over land at 7.7 km altitude showing: **(a)** measured (ARIES) and fitted spectra; **(b)** residual difference between the ARIES-measured spectrum and fitted spectrum; **(c)** Averaging kernels (and degrees of freedom, inset); **(d)** total and component systematic and random error components.

Validation and results from aircraft campaigns

G. Allen et al.

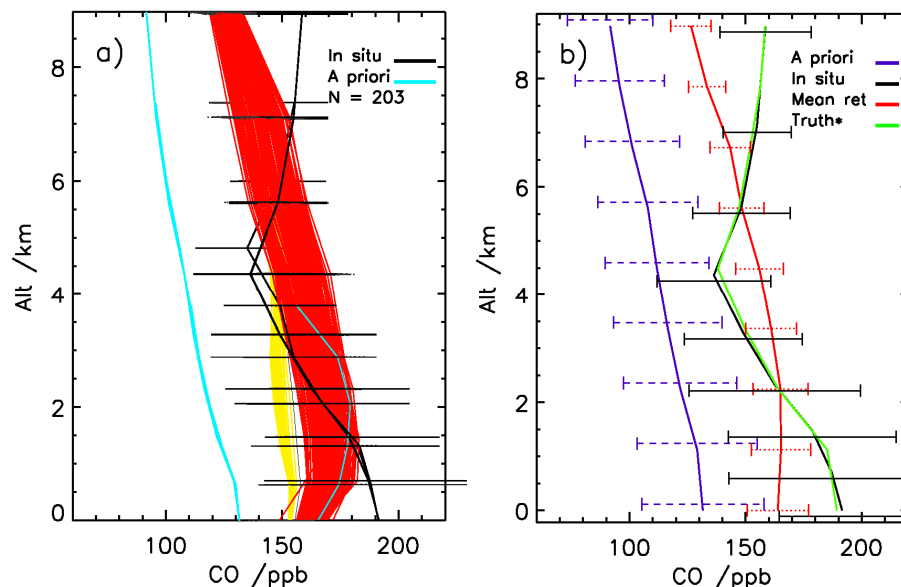


Fig. 11. (a) 203 individual carbon monoxide concentration retrieval profiles across flight B290 colour-coded for observer (flight) altitude. Retrieval uncertainty (total error) is shown as the dotted bars in each case. In situ and a priori profiles are also shown as per legend; **(b)** mean profiles from flight B290 for: retrieved (red), in-situ-measured (black), in-situ average convolved with MARS averaging kernels (green); and a priori (blue). Standard deviations of the measurement variability and a priori are shown as correspondingly-coloured bars at each binned vertical level and the root mean square retrieval uncertainty (total error) is shown by the red bars.

Validation and results from aircraft campaigns

G. Allen et al.

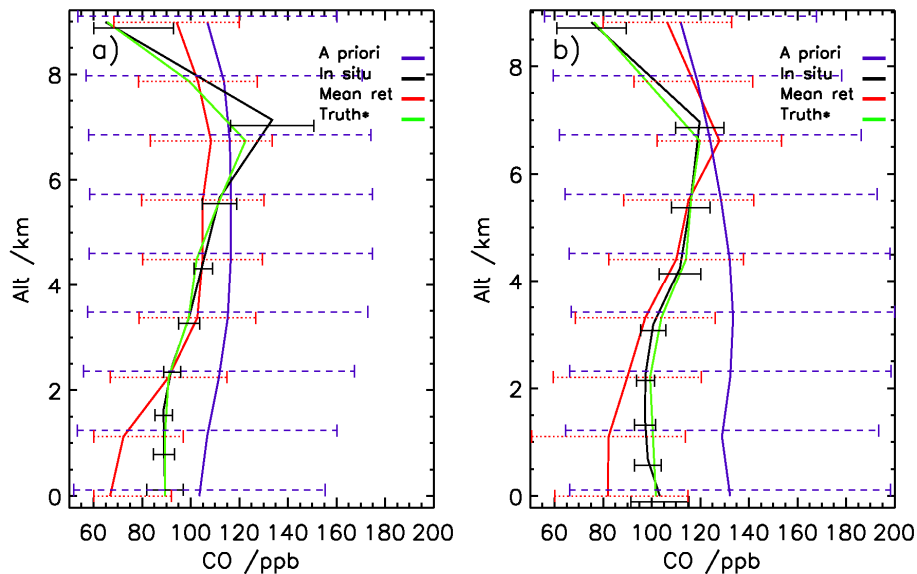


Fig. 12. Carbon monoxide mean profiles as per Fig. 11 but for **(a)** flight B720; and **(b)** flight B724

Title Page

Abstract

Introduction

Conclusions

References

Tables

Figures

◀

▶

◀

▶

Back

Close

Full Screen / Esc

Printer-friendly Version

Interactive Discussion



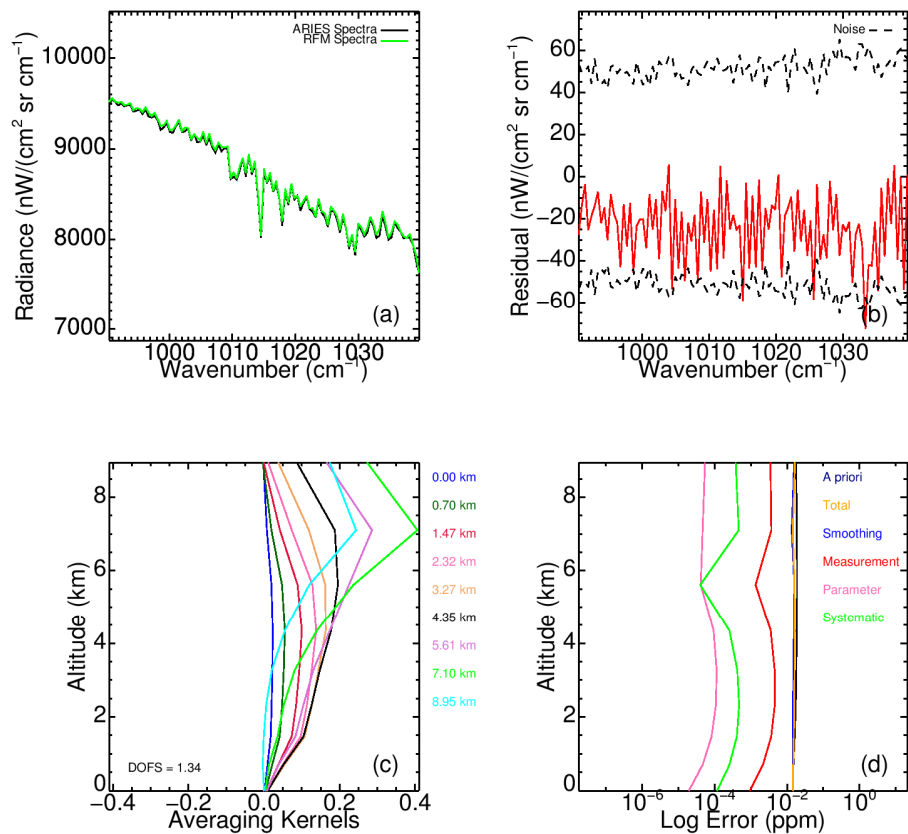


Fig. 13. Example retrieval metrics for O₃ during flight B719 over sea at 8.3 km altitude showing: **(a)** measured (ARIES) and fitted spectra; **(b)** residual difference between the ARIES-measured spectrum and fitted spectrum; **(c)** averaging kernels (and degrees of freedom, inset); **(d)** total and component systematic and random error components.

Validation and results from aircraft campaigns

G. Allen et al.

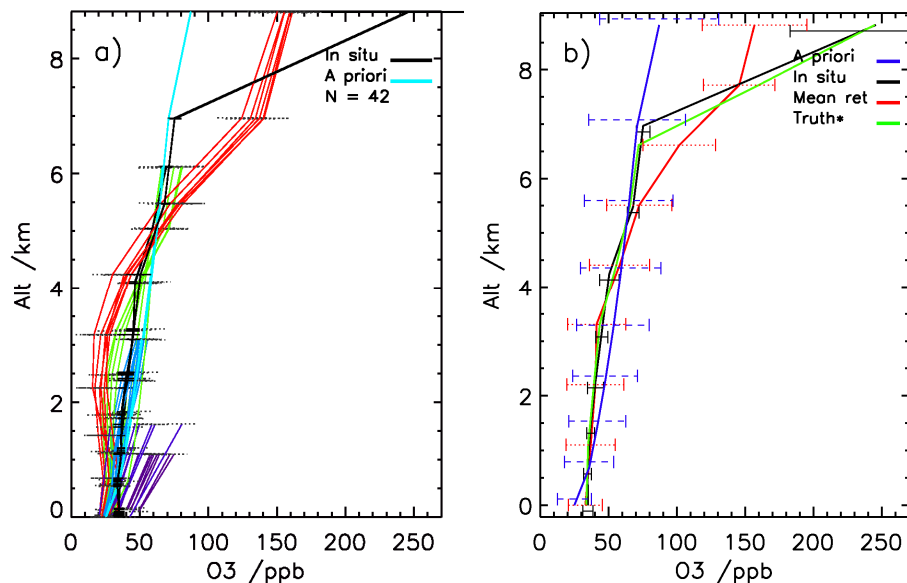


Fig. 14. (a) 42 ozone retrieval profiles from flight B724 colour-coded for flight altitude. Retrieval uncertainty (total error) is shown as the dotted bars in each case. In situ and a priori profiles are also shown as per legend; (b) mean profiles from flight B724 for: retrieved (red), in-situ-measured (black), in-situ average convolved with MARS averaging kernels (green); and a priori (blue). Standard deviations of the measurement variability and a priori are shown as correspondingly-coloured bars at each binned vertical level and the root mean square retrieval uncertainty (total error) is shown by the red bars.

Title Page

Abstract

Introduction

Conclusions

References

Tables

Figures

◀

▶

◀

▶

Back

Close

Full Screen / Esc

Printer-friendly Version

Interactive Discussion



Validation and results from aircraft campaigns

G. Allen et al.

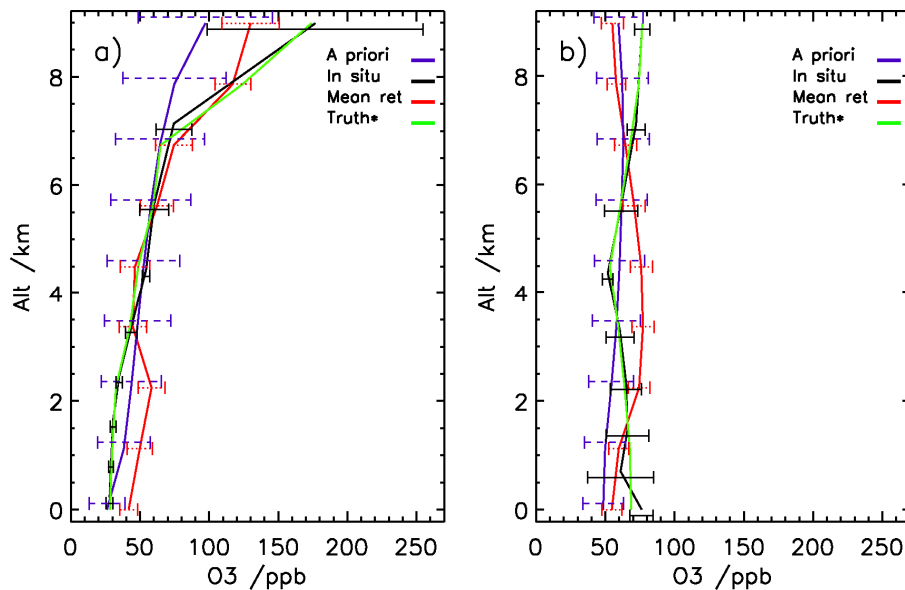


Fig. 15. (a) As for Fig. 14b but for 58 ozone concentration retrieval profiles averaged for flight B720; and (b) as for Fig. 14b but for 191 ozone concentration retrieval profiles averaged for flight B290.

Title Page

Abstract

Introduction

Conclusions

References

Tables

Figures

◀

▶

◀

▶

Back

Close

Full Screen / Esc

Printer-friendly Version

Interactive Discussion

